The Journal of Chemical Physics

Sodium ion transport across the endothelial glycocalyx layer under electric field conditions: A molecular dynamics study

Cite as: J. Chem. Phys. **153**, 105102 (2020); https://doi.org/10.1063/5.0014177
Submitted: 18 May 2020 . Accepted: 17 August 2020 . Published Online: 08 September 2020

Xi Zhuo Jiang, Lumeng Yang, Yiannis Ventikos, and Kai H. Luo

The Journal of Chemical Physics ARTICLE scitation.org/journal/jcp

Sodium ion transport across the endothelial glycocalyx layer under electric field conditions: A molecular dynamics study

Cite as: J. Chem. Phys. 153, 105102 (2020); doi: 10.1063/5.0014177
Submitted: 18 May 2020 • Accepted: 17 August 2020 •
Published Online: 8 September 2020

Xi Zhuo Jiang,[1] Lumeng Yang,[2] Yiannis Ventikos,[1] and Kai H. Luo[1,a)]

AFFILIATIONS

[1] Department of Mechanical Engineering, University College London, Torrington Place, London WC1E 7JE, United Kingdom
[2] Department of Neurology, Huashan Hospital, Fudan University, No. 12 Wulumuqi Zhong Road, Shanghai 200040, People's Republic of China

Note: This paper is part of the JCP Special Topic on Classical Molecular Dynamics (MD) Simulations: Codes, Algorithms, Force fields, and Applications.
[a)] **Author to whom correspondence should be addressed:** k.luo@ucl.ac.uk. **Present address**: Department of Mechanical Engineering, University College London, Torrington Place, London WC1E 7JE, United Kingdom. **Tel.:** +44 (0)20 7679 3916

ABSTRACT

In the present research, the sodium ion transport across the endothelial glycocalyx layer (EGL) under an imposed electric field is investigated, for the first time, using a series of molecular dynamics simulations. The electric field is perpendicularly imposed on the EGL with varying strengths. The sodium ion molarity difference between the inner and outer layers of EGL, Δc, is used to quantify the sodium transport in the presence of the negatively charged glycocalyx sugar chains. Results suggest that a weak electric field increases Δc, regardless of whether the electric field is imposed perpendicularly inward or outward. By contrast, a strong electric field drives sodium ions to travel in the same orientation as the electric field. Scrutiny of the charge distribution of the glycocalyx sugar chains suggests that the electric field modifies the spatial layouts of glycocalyx atoms as it drives the transport of sodium ions. The modification in glycocalyx layouts further changes the inter-molecular interactions between glycocalyx sugar chains and sodium ions, thereby limiting the electric field control of ion transport. The sodium ions, in turn, alter the apparent bending stiffness of glycocalyx. Moreover, the negative charges of the glycocalyx sugar chains play an important role in maintaining structural stability of endothelial glycocalyx. Based on the findings, a hypothesis is proposed regarding the existence of a strength threshold of the electric field in controlling charged particles in the endothelium, which offers an alternative explanation for contrasting results in previous experimental observations.

I. INTRODUCTION

Exactly two decades after the first molecular dynamics (MD) study of simple gases was published in the late 1950s,[1] the MD method was extended to biological macromolecules for the first time.[2] In the pioneering MD work of biomolecules, a bovine pancreatic trypsin inhibitor with 58 amino acid residues in vacuum was simulated for 9.2 ps. With the general availability of computer programs and rapidly increasing computing power, the number of studies using MD to investigate properties and behavior of biosystems has soared. Today, MD simulations can cope with a wide spectrum of biomolecules/atoms, including proteins,[3] lipids,[4] nucleic acid,[5] and carbohydrates.[6] In the meantime, the simulation size has reached the order of millions of atoms,[7,8] and the simulation time has been extended to microseconds.[9] MD simulations offer insights into atomic and molecular behaviors of biomolecules and biosystems that are not always accessible by experimental studies. Moreover, MD simulations of bio-phenomena can be conducted under a non-intrusive *in vivo* environment,[10] without removing the object of interest from the biosystems.

The accessibility to high performance computers and breakthroughs in crystallographic structure determination have empowered MD simulations to tackle increasingly complex and dynamic bio-structures, such as endothelial glycocalyx (EG). The endothelial glycocalyx layer (EGL) is a thin layer covering blood vessels and plays an important role in maintaining vascular health. Dysfunction of the EGL can disrupt vascular homeostasis and cause renal and cardiovascular diseases.[11] A typical endothelial glycocalyx (EG) element comprises proteoglycans with associated glycosaminoglycan (GAG) sugar chains (SCs). The sulfated GAGs are negatively charged, enabling the EG to serve as a microvascular barrier via electrostatic interaction with blood components.[12] Yet, the SCs are highly fragile and dynamic structures, which could cause instability of the endothelial cells when they are studied *in vitro*.[13] To mitigate potential biased conclusions from wet-lab experiments due to the EG instability, MD studies have been undertaken[8,14–17] to investigate the contributions of EG components to its functionality. Indeed, the challenges of using MD to study the EG functionality are manifold: first, a suitable molecular model of EG under physiological conditions is required; second, to cover the sheer size of the EG (with a height of 50 nm–500 nm), the simulation box has to be 10–100 times larger than the typical computational domain (usually smaller than 10 nm) in biomolecule-related MD simulations; third, to fully exploit the unprecedented details contained in the big dataset produced by large-scale MD simulations, efficient and even intelligent post-processing techniques are desired. In the recently published MD studies of EG,[8,14–17] an all-atom molecular model of the EG/flow system was constructed, which contains about 6×10^6 atoms including proteins, lipid membrane, SCs (carbohydrates), ions, and water. Results from these MD studies provided improved understanding of the roles of EG in controlling microvascular mass transport[15,17] and mechanotransduction.[16] Among other findings, the role of charges in maintaining protein–lipid interactions was revealed by altering charge distributions of proteins.[18] The effects of external electric fields in a variety of applications including biosystems have been investigated using MD and reviewed recently.[19]

Electric fields with physiological strengths play a pivotal role in wound healing and tissue regeneration (as reviewed in Ref. 20). Both the endogenous and exogenous electric fields have great significance in physiology and disease treatment. *In vivo*, endogenous direct current (DC) electric fields occur in the form of epithelial transcellular or neuronal field potentials.[21] *In vitro*, cells move directionally as a response to exogenous electric fields. The directional movement of organs, tissues, or cells guided by an electric field or current is termed *galvanotaxis* or *electrotaxis*.[22] The galvanotaxis feature of cells or organisms lends the possibility to use the electric field as a treatment for patients. For example, an applied electric field can stimulate and direct regeneration of most myelinated axons in the damaged spinal cord and, thus, can be used in treating patients with spinal cord injuries.[23] The effects of an electric field on the bending of the negatively charged EG were also experimentally studied.[24] It is noted that most galvanotaxis studies are performed by experiments due to the complicity of biomolecules.

In the light of these facts, we would like to post three questions: Can an electric field be used to control mass transport (e.g., sodium ion transport) across the EGL and potentially treat conditions induced by the loss of EGL microvascular permeability? Can MD simulations serve as an alternative to *in vivo* experiments to test such a hypothesis? If so, what new insights will MD simulations provide that are not easily accessible by experiments? To answer these questions, Na^+ transport across the EGL under varying electric field conditions is investigated, for the first time, by a series of sophisticated MD simulations. Cases with varying electric field strengths and orientations are performed to reproduce Na^+ behavior in the presence of the negatively charged glycocalyx. In Sec. II, the molecular model of endothelial glycocalyx is described; and details of the MD methodology and simulation cases are provided. In Sec. III, the effects of the electric field on Na^+ transport are studied first, followed by the influence of the electric field on charge distribution and physical properties of EG. In Sec. IV, the results are discussed in the context of electric field–EG relationship and galvanotaxis. Strategies of using an electric field to control EG mass transport are also discussed. A summary of this research is given, and future work is suggested in Sec. V.

II. METHODS

A. Molecular model of endothelial glycocalyx

The focus of this research is a small patch of the endothelial cell membrane, as illustrated in Fig. 1. The whole domain is split by the membrane into two compartments: the lumen where the blood flow passes by, and the cytoplasm, which is the inner part of the endothelial cells. The SCs of the EG, anchored to the core proteins (proteoglycans), are exposed to the blood flow in the lumen. An array of core proteins is embedded into the membrane. The space between any two adjacent individual proteins is about 200 Å, which is in accordance with experimental observations.[25]

A POPC (1-palmitoyl-2-oleoyl-sn-glycero-3-phosphocholine) lipid bilayer is used to mimic the membrane. Syndecan-4 protein and heparan sulfate (HS) chains are adopted in the construction of a simplified glycocalyx element as syn-4 is ubiquitously expressed and mediates numerous critical cellular processes such as mechanotransduction,[26] and HS chains account for the majority of the GAG

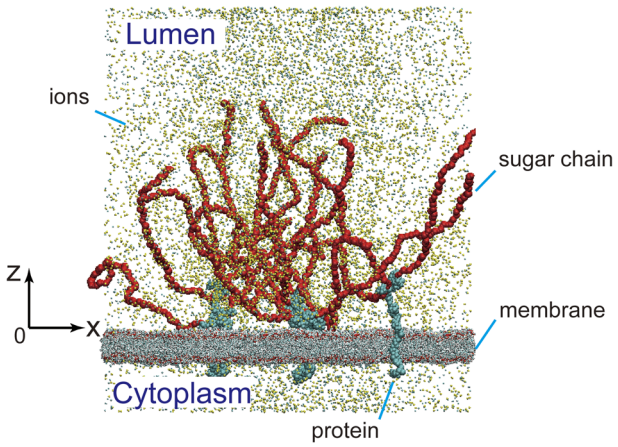

FIG. 1. Initial configuration of the system. Water molecules are not shown for clarity. The electric field is imposed in the *z* direction.

chains.[27] One hundred sugar residues (with four sugar residues as a linker to syndecan-4) are used to build one EG sugar chain, among which four residues are covalently attached to the syndecan-4 protein, and the remaining 48 disaccharide units form the main body of an EG sugar chain. The detailed sequence of the sugar residues is introduced in a previous study.[7] The total charge of an HS chain in this research is −89 e (e is the unit charge), with −88 e from the main body, and $-e$ from the linker residues.[7] The detailed charge distribution is provided in the supplementary material. A simulation unit contains three syndecan-4 proteins and 18 HS chains.

The entire system is solvated in a NaCl aqueous solution with a concentration of 0.1M. Together with Na^+ added to neutralize the negatively charged EG sugar chains, the total Na^+ molarity is about 0.15 M, and the Cl^- molarity is 0.1 M. The values of Na^+ and Cl^- ions are both in a physiological range.[28] In accordance with previous studies, the simulation unit is set to a hexagonal prism[29,30] with an area of 820 nm^2 and height of 72 nm. The flow/EG system comprises 5 800 000 atoms in total. For clarity, water molecules are not shown in Fig. 1.

B. Case setups

To investigate the mechanism whereby the electric field affects sodium transport, a series of cases are designed, as listed in Table I. Previous studies[24,31] suggest that an electric field of ~100 V/m is of physiological relevance that could cause response from cells or biomolecules. Case I is a non-electric-field case for comparison, representing a normal glycocalyx situation without being treated by a field. In cases II to IV, an electric field of 100 V/m is individually applied in the orientation perpendicular to the lipid membrane. Cases II and III are designed to show the effects of electric field orientation on Na^+ transport with two opposing electric field orientations (i.e., reversing polarity). In case IV, the negative charges of the endothelial glycocalyx SCs are artificially switched off. Comparison between cases III and IV will reveal the role of the SC charges in EGL microvascular physiology. Cases with an electric field of weaker (10 V/m, cases V and VI) and stronger (200 V/m, cases VII and VIII) strengths are also included.

C. MD simulation details

The TIP3P water model[32] is adopted to simulate water molecules. To mimic flow, external forces are imposed on oxygen atoms of water molecules, and the flow simulation lasts for a physical time of 30 ns.[8] Afterward, the electric field or the modification of EG sugar chain charges is implemented as per Table I for a physical time of 4 ns. In the 4-ns simulations, external forces are no longer imposed on water oxygens, and the flow is maintained by the inertia. As the interest of this study is the effects of an electric field on sodium transport, the last frame of the 30-ns flow simulation is set as the time origin (i.e., $t = 0$). The interactions among the biomolecules are calculated by a CHARMM biomolecular force field.[33] The temperature is maintained at 310 K with a Lowe–Andersen thermostat. The velocity Verlet integration method[34] is used to advance the positions and velocities of the atoms in time. A 2-fs time step and the particle mesh Ewald[35] electrostatics with a grid density of $1/Å^3$ are used. The SETTLE algorithm[36] was used to enable the rigid bonds connected to all hydrogen atoms. The van der Waals interactions were calculated using a cutoff of 12 Å with a switching function starting at 10 Å.[7] The open source platform NAMD 2.9[37] was used to conduct the MD simulations.

The visualization of the molecular structures was performed by the VMD[38] package. All parallel simulations and non-visualized post-processing were conducted on ARCHER, UK's national supercomputing service.

TABLE I. Case setups in this research.

Cases	Electric field (V/m)	EG sugar chain charges
I	0	Intact
II	$+z$, 100	Intact
III	$-z$, 100	Intact
IV	$-z$, 100	Off
V	$+z$, 10	Intact
VI	$-z$, 10	Intact
VII	$+z$, 200	Intact
VIII	$-z$, 200	Intact

D. Post-processing

To investigate the spatial distribution of charges, a domain originating from the upper membrane surface (origin in Fig. 1) with a height of 50 nm is the region of interest for post-processing. This domain is sliced into 25 equal bins, and the quantities are averaged within each bin. Data are sampled every 0.02 ns.

III. RESULTS

A. Effect of electric field on Na^+ transport

To measure sodium ion transport across the EGL, a molarity difference of Na^+ ions between the two thin layers below and above the glycocalyx sugar chain rich regions is defined as follows:

$$\Delta c = c_b - c_a = \frac{n_b}{V_{b,water}} - \frac{n_b}{V_{a,water}}. \quad (1)$$

In Eq. (1), c is the Na^+ molarity, n is the number of Na^+ ions, and V represents the volume of water. The subscripts b and a represent the thin layers below and above the SC-rich region, respectively, and the heights of both thin layers are 4 nm. Our previous studies[15,17] have demonstrated that c_b is greater than c_a, so Δc is greater than 0. Figure 2 shows the comparisons of average molarity differences over time among the cases listed in Table I.

In Fig. 2(a), when the $+z$-direction electric field strength increases, two opposite trends of Δc changes have been identified: when a strong electric field of 200 V/m is imposed, the molarity difference, Δc, is attenuated as more Na^+ ions are transported from the bottom region to the top region under the electrostatic force from the electric field; however, when a weak (10 V/m) or moderate (100 V/m) electric field is imposed, increases in Δc are observed. When an electric field is applied, the negatively charged SCs move in an opposite direction against Na^+ ions. The changes in the relative positions directly result in the inter-molecular interaction changes

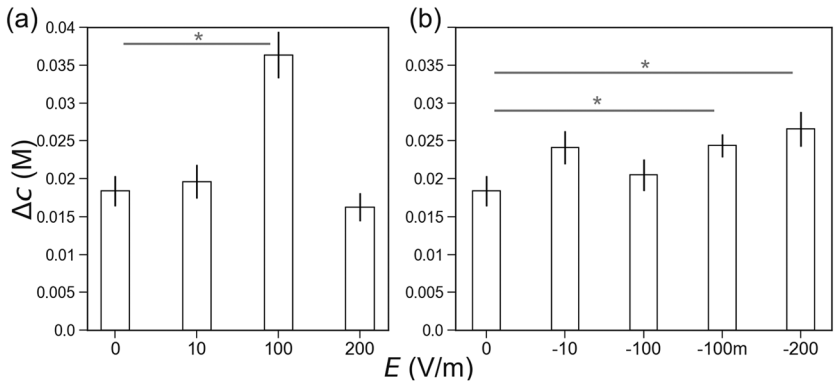

FIG. 2. Comparisons of average molarity difference of Na^+ among cases with varying electric field strengths and orientations. (a) Comparisons among cases with no electric field and those with an electric field imposed on the +z direction. (b) Comparisons among cases with no electric field and those with an electric field imposed on the −z direction. −100m is the case (case IV) where the negative charges of SCs are artificially switched off. T-tests are used to check the statistical significance between cases with and without an electric field. ∗ represents $p < 0.05$.

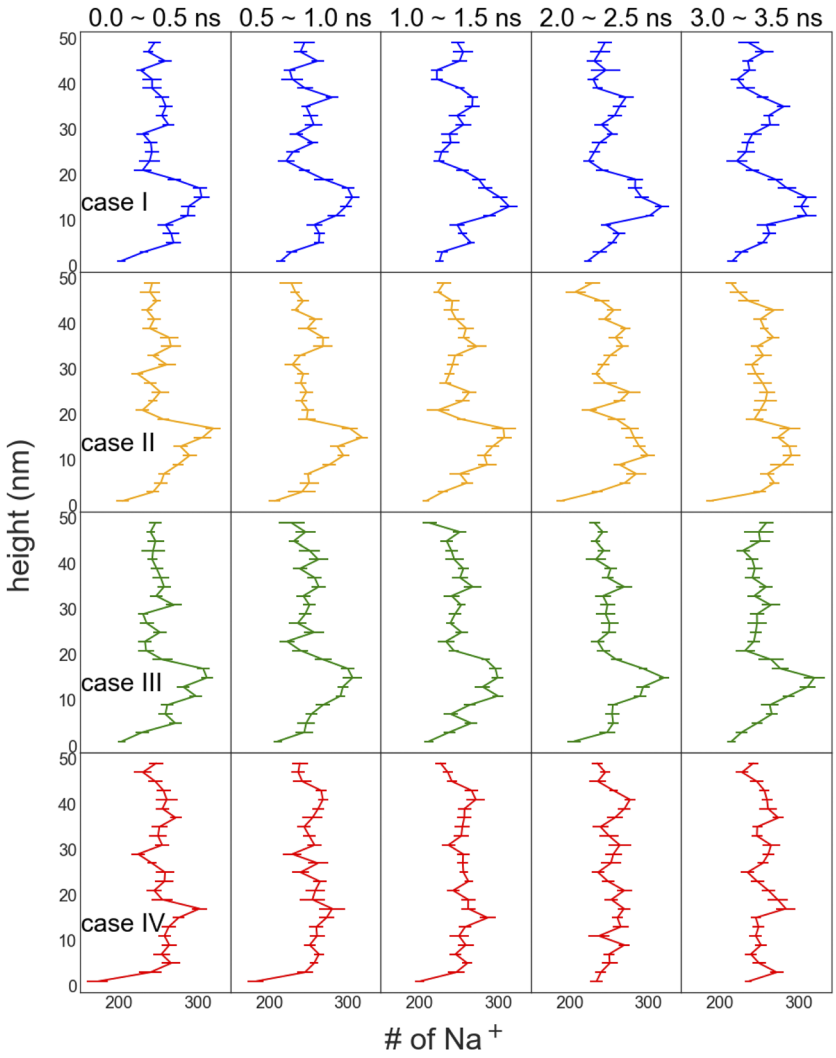

FIG. 3. Na^+ spatial distributions along the height in cases I to IV.

between SCs and ions. When a weak electric field is imposed on the system, the inter-molecular interactions from the negatively charged SCs on Na^+ ions overcome the electric field and alter the movement of Na^+ ions from outward to inward, thereby leading to the increase in Δc. The negative charges of EGL, therefore, result in the existence of an optimal electric field strength for using an electric field to control the Na^+ transport over the EGL. The optimal strength can be interpreted by regarding water and glycocalyx as continuum. For Na^+ ions, the electrostatic force from the electric field ($F_E = qE$, and q is the total charges of Na^+ ions) is a driving force, and the electrostatic forces from SCs (F_{SC}) and Cl^- ions (F_{Cl}) are drag forces. When the electric field is just applied, F_{SC} and F_{Cl} are greater than F_E due to the compact spatial distribution of the ions. Under the driving forces from the electric field, Na^+ ions gradually move away from the negatively charged particles, and F_{SC} and F_{Cl} decrease accordingly. The time when F_E dominates the motion of Na^+ ions depends on the electric field strength applied. Thus, to ensure Na^+ ion transport at a required rate, the strength of an electric field should be carefully adjusted, and the corresponding electric field is of the optimal strength.

In Fig. 2(b), the application of a downward electric field drives the Na^+ transport from outside the SC-rich region to inside in all the applied electric field strengths. It is noteworthy that the effects of the changing inter-molecular interactions from the negatively charged SCs on Na^+ ions still exist in these cases. The existence is demonstrated by comparing Δc increases in the −100 (i.e., case III in Table I) and −100 m (case IV in Table I) cases: in case IV where the negative charges of glycocalyx SCs are switched off, the increase in Δc compared with the $E = 0$ case indicates that Na^+ transport in the same direction as the electric field, as expected; when negative charges of SCs are involved, a smaller increase in Δc in case III is spotted, which implies that the inter-molecular interaction changes from SCs have jeopardized Na^+ transport. Due to the finite lengths and the stretching structures of the SCs, the upward movement of SCs will equilibrate at a relatively fixed position, which means that the effect of the SCs to modify Na^+ ion transport via inter-molecular interactions is limited. The limited effects from the SCs are insufficient to alter the Na^+ movement driven by the electric field, which accounts for the elevated Δc in all electric field cases in Fig. 2(b).

B. Effect of electric field on Na^+ spatial distributions

The effect of an electric field on Na^+ spatial distribution is further investigated. Given that water molecules are electrically neutral and the number of water molecules is far greater than Na^+ ions, the volumes of water in Eq. (1) are assumed constant. Thus, changes in Δc in the electric field cases are mainly attributed to the alteration in Na^+ spatial distribution by the electric field. Follow-on analysis will focus on cases with an electric field of 100 V/m, and as such, strength is physiological, and Fig. 2(a) suggests that more complicated dynamics have occurred under such an electric field strength. For comparison, case I is also included in the analysis that follows.

Na^+ number distributions along the height in cases I to IV are illustrated in Fig. 3. In each panel, data are averaged over 0.5 ns. At the initial stage (0.0 ns–0.5 ns) when the electric field is just applied, cases I to III have almost the same Na^+ number distributions. During this period, Na^+ ions and SCs are close to each other, and Na^+ number distributions are mainly determined by the SC layouts. As the electric field continues to act on the system, Na^+ ions and SCs move away from each other. The driving force from the electric field on Na^+ ions, then, gradually overcomes the drag force from SCs, and Na^+ ion transport is dominated by the electric field. At the closing stage (3.0 ns–3.5 ns), changes in Na^+ number distributions follow different trends: in case II, Na^+ ions move from the near-lipid-membrane region to the lumen, and the number peak ($h = 12$ nm–16 nm) is weakened; in case III, Na^+ ions travel from the lumen to the near-lipid-membrane region and cumulate inside the EGL, and an enhanced peak can be observed at $h = 12$ nm–16 nm. Compared with case I, the distribution curves in cases II and III have smoother profiles in the $h > 20$ nm region as the simulation goes, which can be attributed to the movement of Na^+ ions as well. In case IV where the charges of SCs are set to 0, the motion of Na^+ ions is controlled by the electric field, and a relatively even distribution is observed.

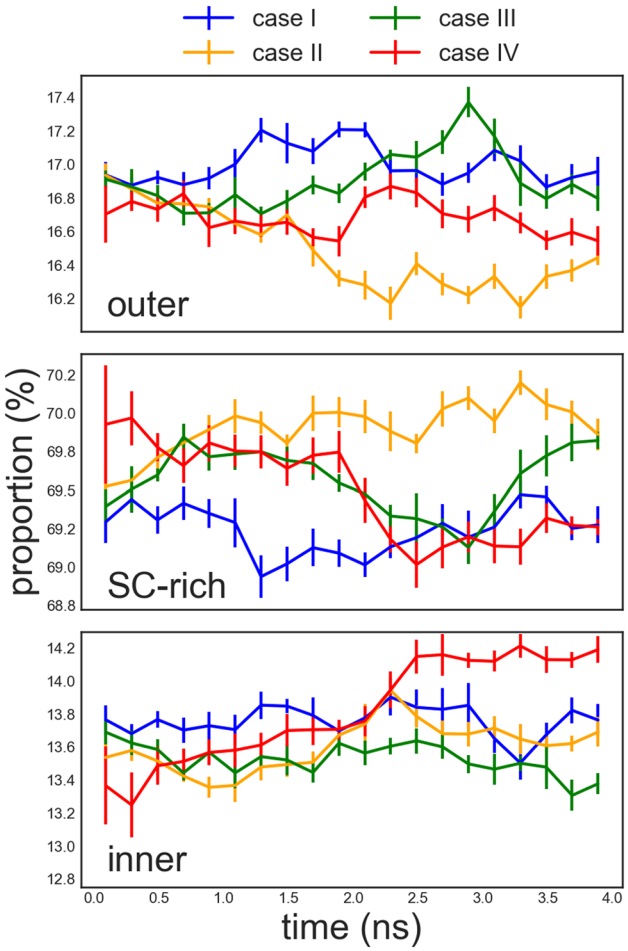

FIG. 4. Proportions of Na^+ ions in three regions: an inner region below the SC-rich region, within the SC-rich region, and an outer region above the SC-rich region. Each point in this figure is time-averaged over 0.2 ns.

To further explore the transport of Na^+ ions, the domain above the lipid membrane is divided into three regions: the region from the origin to 8 nm in height is the inner region, 8 nm to 44 nm is the SC-rich region, and 44 nm and upward is the outer region. The proportions of Na^+ ions in individual regions are calculated and shown in Fig. 4. In case II, Na^+ ions travel from the outer region to the SC-rich and inner regions, which implies that the intermolecular interactions from the SCs on Na^+ ions have overcome the driving force from the upward electric field. Comparisons between cases III and IV further demonstrate that the electrostatic interactions from SCs significantly alter the Na^+ transport direction across the EGL.

C. Effect of electric field on SC spatial distributions

As the electrostatic interactions from SCs significantly impact Na^+ transport, the movement of the negatively charged SCs is scrutinized. The charge distributions of SCs at all the sampling frames are calculated. As shown in Figs. 5(a)–5(c), the imposition of an electric field affects the motion of the SCs as it drives the movement of Na^+ ions. To gauge the motion of SCs, a center of charge (CoC) in the SC-rich region is defined in Eq. (2). By recording the CoCs at each frame, the movement of SCs can be monitored,

$$\mathrm{CoC} = \frac{\int hdq}{\int dq} = \frac{\sum\limits_{i\in SC} h_i q_i}{\sum\limits_{i\in SC} q_i}. \tag{2}$$

In Eq. (2), h_i is the position of the ith layer in the SC-rich region and q_i is the charge of SCs in the ith layer. As illustrated in Fig. 5(d), the electric field drives the motion of negatively charged SCs. Apparently, in case III, the elevated CoC demonstrates that the downward electric field has imposed an upward impulse on SCs. Both cases I and II witness the falling of CoCs throughout the simulations. However, in case I, the CoC first climbs to a peak value and, then, falls to a lower position; by contrast, in case II, a dramatic drop of CoC is first spotted at the beginning stage, and afterward, the CoC oscillates around a fixed position between 18.4 nm and 18.5 nm. The different trends in the early stages indicate that the electric field directs the motion of SCs as it drives Na^+ movement.

D. Effect of electric field on glycocalyx deformation

Snapshots of deformations of three randomly selected SCs in cases I to IV are illustrated in Fig. 6. The conformational differences in the four cases reveal a direct consequence of the imposition of the electric field on EGL—to distort the negatively charged SCs.

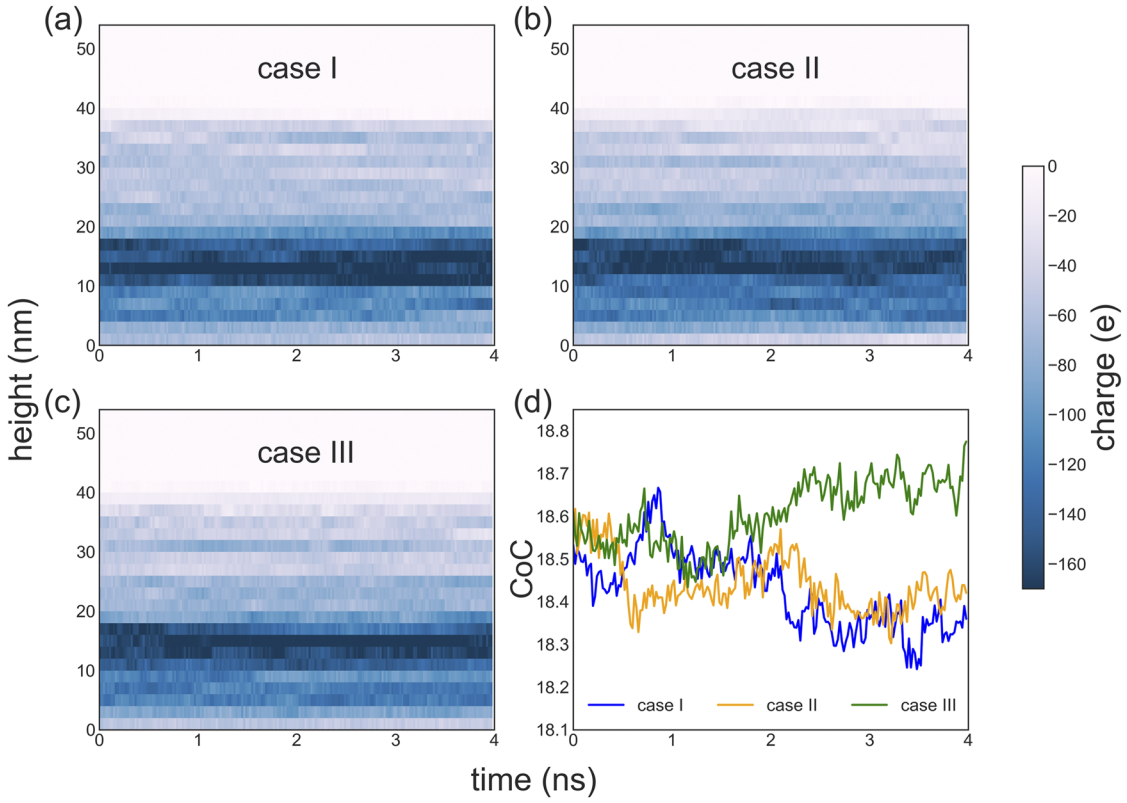

FIG. 5. Charge distributions and time evolution of Center of Charges (CoCs) of sugar chains. (a) Charge distributions of sugar chains in case I. (b) Charge distributions of sugar chains in case II. (c) Charge distributions of sugar chains in case III. (d) Time evolution of CoCs of cases I to III.

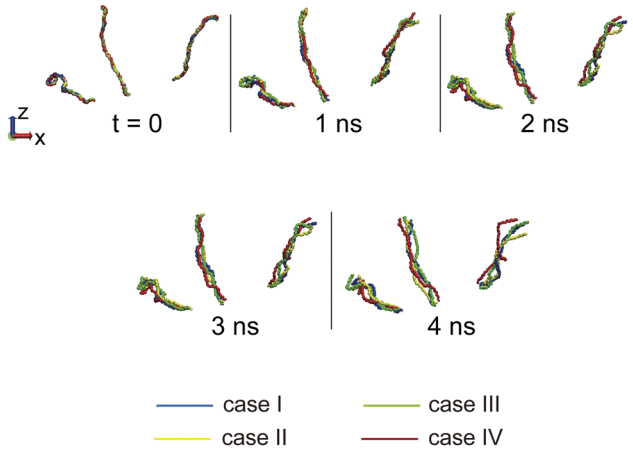

FIG. 6. Snapshots of deformations of three randomly selected sugar chains (front view).

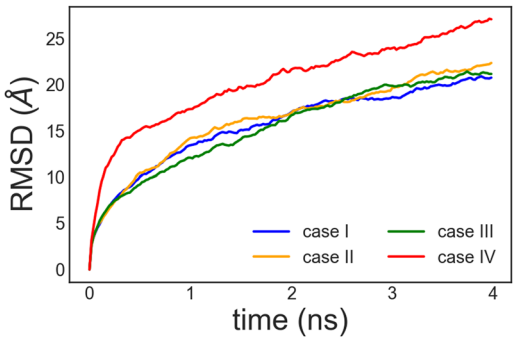

FIG. 7. Root-mean-square deviations (RMSDs) of sugar chains in cases I to IV. Cases II and III have slightly higher RMSDs at the concluding stage of the simulations, which indicates that the electric field distorts the SCs. The large RMSD changes in case IV suggest the importance of the negative charges of SCs in maintaining structural stability.

The deformation or conformational changes of SCs are the position changes of the constitute atoms. To gauge the deformation, a root-mean-square deviation (RMSD) of atomic positions as defined in the following equation is used:

$$\mathrm{RMSD} = \left(\frac{\sum_{i=1}^{N} w_i \left\| \mathbf{x}_i - \mathbf{y}_i \right\|^2}{N \sum_{i=1}^{N} w_i} \right)^{1/2}. \tag{3}$$

In Eq. (3), $\mathbf{x}$ and $\mathbf{y}$ are two consecutive structures of SCs; N is the number of atoms of interest, and in this study, non-H atoms from all the 18 sugar chains are counted with a value of 25 200; and w_i is a weight coefficient and identical among atoms in this research. RMSDs of cases I to IV are compared in Fig. 7. Cases II and III have slightly higher RMSDs than their case I counterpart at the concluding stage of the simulations, which corroborates the distortion of SCs by the electric field. Interestingly, case IV has the greatest deformation, affirming that the negative charges play a role in maintaining the structural stability of glycocalyx.

E. Effect of electric field on apparent bending stiffness

To describe the resistance of the glycocalyx to the external forces, apparent bending stiffness (BS) of SCs is further investigated. The BS can be linked to persistence length (L_p) by the following equation:[39]

$$L_p = \frac{\mathrm{BS}}{k_B T}. \tag{4}$$

In Eq. (4), k_B is the Boltzmann constant, and T is the temperature. L_p can be obtained by solving the following equation:[40]

$$\left\langle l_{be}^{\,2} \right\rangle = 2L_c L_p - 2L_p^{\,2}\left[1 - \exp(-L_c/L_p)\right]. \tag{5}$$

In Eq. (5), $\langle l_{be}^{\,2} \rangle$ is the averaged square end-to-end distance, and L_c is the contour length of SCs with a value of 516 Å in this study. End-to-end distances are measured and averaged among all the SCs at every time frame. Incorporating L_p from Eq. (5) into Eq. (4), then, gives the apparent BS. Entropic stretching of SCs can result in changes in the end-to-end distance. To mitigate the influence of entropic stretching and manifest the effects of an electric field or "muted" charges on the bending stiffness, the end-to-end distances and BSes are further averaged over all the time frames in the 4-ns simulations. Figure 8 shows the comparisons of the average end-to-end distances and apparent BSes among cases I to IV. The electric field imposes manifold influences on the end-to-end distance and the apparent BS of SCs: first, it can directly modify the atomic positions of SC components via electrostatic forces, thereby modifying the end-to-end distance and the apparent BS; it can also

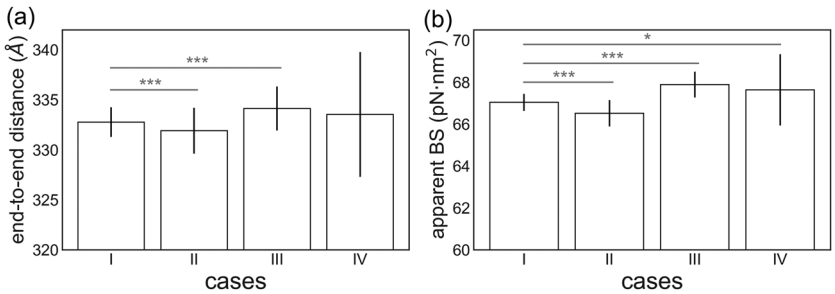

FIG. 8. Average end-to-end distance of glycocalyx sugar chains and the corresponding apparent binding stiffness (BS) in cases I to IV. (a) Average end-to-end distances in the four cases. (b) Apparent BS in the four cases. T-tests are used to check the statistical significance between cases with and without an electric field. $^*p < 0.05$ and $^{***}p < 0.001$.

alter the spatial distributions of the surrounding ions with their interactions with SCs being changed. As illustrated in Fig. 8, the orientation of the electric field affects the average end-to-end distance and the apparent BS of SCs: compared with case I, the $+z$-direction electric field of case II shortens the average end-to-end distance of SCs and impairs the apparent BS, while the $-z$-direction electric field in case III extends the SCs and enhances the BS. Comparisons between cases III and IV further validate the role of negative charges in maintaining the BS.

IV. DISCUSSION

When an electric field is applied over the endothelium, it affects the dynamics of all the charged atoms/particles inside the EGL. In this study, the electric field modifies the atom positions of SCs as it drives the Na^+ ion transport. Figure 9 summarizes the relationship among the electric field, the negatively charged SCs, and Na^+ ions. The inter-molecular interactions between SCs and Na^+ comprise van der Waals and electrostatic interactions. The changes in SC positions by the electric field consequently cause the inter-molecular interaction changes between SCs and Na^+ ions. As the SCs and Na^+ ions are of opposite charges, the attractive electrostatic forces, then, form a drag force to impede the oriented transport of Na^+ ions driven by the electric field. The Na^+ ions, in turn, alter the apparent properties of SCs via the varied ion spatial distribution.

Here, we propose a hypothesis regarding the existence of a threshold of the electric field in driving the oriented movement of charged particles in the endothelium. Below the threshold, the hindrance from the endothelium increases with the electric field strength. In Fig. 2, the strength threshold of the electric field to control Na^+ transport is a value between 100 V/m and 200 V/m, and the 100 V/m case has a stronger interference in Na^+ transport than its 10 V/m counterpart. This hypothesis can also be extended to the galvanotaxis of cells in order to provide explanations for some contradicting results in the literature. For example, previous studies showed that a weak electric field of 10 V/m could produce galvanotaxis in cells only in a few minutes;[41] by contrast, a strong electric field of 1500 V/m took about 25 min to achieve an equilibrium redistribution of charged surface proteins on rat basophilic leukemia cells.[42] According to our hypothesis, a strong electric field could result in great resistance from the surface glycocalyx as it drives cells. To overcome the large resistance, additional energy, which means longer exposure time to the electric field, is required.

Indeed, the hindrance from the negatively charged glycocalyx on Na^+ transport also has a favorable impact. As shown in Fig. 2, increases in Δc are always found in cases with weak electric fields (10 V/m and 100 V/m), independent of the directions of electric fields. This feature would benefit the application of both alternating current (AC) and DC electric fields in Na^+ transport control, especially when a consistent Na^+ transport direction is needed. In an AC electric field with a delicately designed strength, the direction of Na^+ transport can remain unchanged when the direction of the electric field is changed. When a DC electric field is applied to the blood vessels, the roughly cylindrical geometry of the blood vessels [Figs. 10(a) and 10(b)] and their arbitrary orientations in 3D [Fig. 10(c)] cause diverging effects on Na^+ movement. If there were no charges of SCs, the electric field would drive the Na^+ transport toward the lumen in the upper half of the blood vessel, but drive Na^+ ions away from the lumen in the lower half, as schematically shown in Fig. 10(a). According to our results, in weak electric-field conditions,

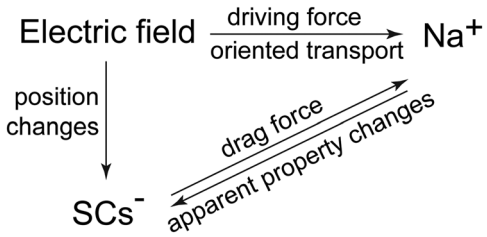

FIG. 9. Relationship among Na^+ ions, SCs, and the electric field. The electric field is the driving force of Na^+ transport and changes the SC conformations as well. The electrostatic interaction from SCs jeopardizes the oriented movement of Na^+ ions by the electric field. The changing Na^+ distribution, in turn, alters apparent properties of SCs.

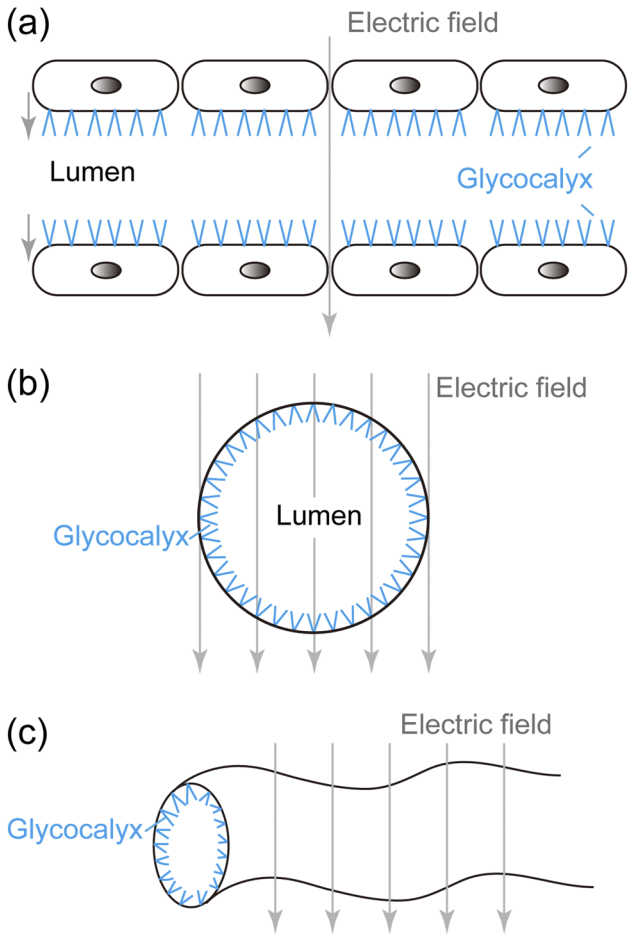

FIG. 10. Schematic of blood vessels under a DC electric field. (a) Cross section along a blood vessel. (b) Radial cross section. (c) A tortuous blood vessel.

the existence of the negative charges of SCs will reconcile the diverging effects and maintain a consistent Na^+ transport direction to the lumen.

V. CONCLUSIONS

In this research, the sodium ion transport across the EGL under the influence of an electric field is investigated. To study the effects of electric field strengths on Na^+ movement, a series of molecular dynamics simulations are conducted. The electric field is perpendicularly imposed on the EGL with strengths of 10 V/m, 100 V/m, and 200 V/m, respectively. The Na^+ molarity difference between the inner and outer regions of EGL, Δc, is used to quantify Na^+ transport. Compared with the situation without an electric field, a weak electric field (10 V/m and 100 V/m) increases Δc independent of the electric field orientation. By contrast, in the presence of a strong electric field (200 V/m), Na^+ ions travel in the same orientation of the electric field. The electric field modifies the spatial distributions of SCs as it drives the transport of Na^+ ions. The modification in SC layouts would change the inter-molecular interactions between SCs and Na^+, thereby limiting the control of Na^+ ions via the electric field. The Na^+ ions, in turn, alter the apparent bending stiffness of SCs via the varied spatial distribution. Results also indicate that the negative charges of SCs play an important role in maintaining structural stability of glycocalyx.

This research adds unique atomic insight into the electric field control over EGL ion transport and could facilitate the design of electric-field-assisted therapeutic strategies to cure cardiovascular diseases. In future work, it is desirable to investigate the effects of an electric field with parallel orientations to EGL on microvascular permeability and mechanotransduction.

SUPPLEMENTARY MATERIAL

Charge distribution of sugar residues is provided in the supplementary material.

AUTHORS' CONTRIBUTIONS

X.Z.J. and L.Y. contributed equally to this work.

ACKNOWLEDGMENTS

Funding from the U.K. Engineering and Physical Sciences Research Council (EPSRC) under the "U.K. Consortium on Mesoscale Engineering Sciences (UKCOMES)" (Grant No. EP/R029598/1) is gratefully acknowledged.

DATA AVAILABILITY

The data that support the findings of this study are available within the article and its supplementary material.

REFERENCES

[1] B. J. Alder and T. E. Wainwright, J. Chem. Phys. **27**, 1208 (1957).
[2] J. A. McCammon, B. R. Gelin, and M. Karplus, Nature **267**, 585 (1977).
[3] M. Karplus and J. Kuriyan, Proc. Natl. Acad. Sci. U. S. A. **102**, 6679 (2005).
[4] S. E. Feller, Curr. Opin. Colloid Interface Sci. **5**, 217 (2000).
[5] T. E. Cheatham III and P. A. Kollman, Annu. Rev. Phys. Chem. **51**, 435 (2000).
[6] E. Fadda and R. J. Woods, Drug Discovery Today **15**, 596 (2010).
[7] E. R. Cruz-Chu *et al.*, Biophys. J. **106**, 232 (2014).
[8] X. Z. Jiang *et al.*, J. R. Soc., Interface **14**, 20170780 (2017).
[9] E. A. Cino *et al.*, PLoS One **6**, e27371 (2011).
[10] M. Karplus and J. A. McCammon, Nat. Struct. Biol. **9**, 646 (2002).
[11] T. J. Rabelink and D. de Zeeuw, Nat. Rev. Nephrol. **11**, 667 (2015).
[12] C. S. Alphonsus and R. N. Rodseth, Anaesthesia **69**, 777 (2014).
[13] M. J. C. Dane *et al.*, Am. J. Physiol.:Renal Physiol. **308**, F956 (2015).
[14] X. Z. Jiang *et al.*, Comput. Fluids **173**, 140 (2018).
[15] X. Z. Jiang, K. H. Luo, and Y. Ventikos, Front. Physiol. **9**, 1667 (2018).
[16] X. Z. Jiang, K. H. Luo, and Y. Ventikos, Acta Physiol. **228**, e13376 (2020).
[17] X. Z. Jiang, Y. Ventikos, and K. H. Luo, Am. J. Physiol.: Heart Circ. Physiol. **317**, H104 (2019).
[18] X. Z. Jiang *et al.*, Ann. Biomed. Eng. **48**, 357 (2020).
[19] N. J. English and C. J. Waldron, Phys. Chem. Chem. Phys. **17**, 12407 (2015).
[20] G. C. Gurtner *et al.*, Nature **453**, 314 (2008).
[21] M. E. Mycielska and M. B. A. Djamgoz, J. Cell Sci. **117**, 1631 (2004).
[22] B. Cortese *et al.*, Integr. Biol. **6**, 817 (2014).
[23] R. B. Borgens, Neuroscience **91**, 251 (1999).
[24] F. X. Hart and J. R. Palisano, Bioelectromagnetics **38**, 482 (2017).
[25] K. P. Arkill *et al.*, Biophys. J. **101**, 1046 (2011).
[26] A. Elfenbein and M. Simons, J. Cell Sci. **126**, 3799 (2013).
[27] S. S. Deepa *et al.*, J. Biol. Chem. **279**, 37368 (2004).
[28] S. Fuggle, *Clinical Biochemistry Reference Ranges Handbook V1.8* (East Sussex Healthcare, NHS Trust, East Sussex, 2018), p. 1.
[29] S. Weinbaum *et al.*, Proc. Natl. Acad. Sci. U. S. A. **100**, 7988 (2003).
[30] Y. Zeng *et al.*, Am. J. Physiol.: Heart Circ. Physiol. **305**, H811 (2013).
[31] F. X. Hart, Bioelectromagnetics **29**, 447 (2008).
[32] W. L. Jorgensen *et al.*, J. Chem. Phys. **79**, 926 (1983).
[33] A. D. Mackerell *et al.*, J. Phys. Chem. B **102**, 3586 (1998).
[34] M. P. Allen and D. J. Tildesley, *Computer Simulation of Liquids* (Clarendon Press, Oxford, 1987).
[35] T. Darden, D. York, and L. Pedersen, J. Chem. Phys. **98**, 10089 (1993).
[36] S. Miyamoto and P. A. Kollman, J. Comput. Chem. **13**, 952 (1992).
[37] J. C. Phillips *et al.*, J. Comput. Chem. **26**, 1781 (2005).
[38] W. Humphrey, A. Dalke, and K. Schulten, J. Mol. Graphics **14**, 33 (1996).
[39] F. Gittes *et al.*, J. Cell Biol. **120**, 923 (1993).
[40] L. M. J. Kroon-Batenburg *et al.*, J. Phys. Chem. B **101**, 8454 (1997).
[41] L. Huang *et al.*, J. Cell. Physiol. **219**, 162 (2009).
[42] T. A. Ryan *et al.*, Science **239**, 61 (1988).